UC San Diego
UC San Diego Previously Published Works

Title

Single-cell analysis in hypersaline brines predicts a water-activity limit of microbial anabolic activity.

Permalink

https://escholarship.org/uc/item/02g0w8w7

Journal

Science Advances, 9(51)

Authors

Pontefract, Alexandra
Elbon, Claire
Glass, Jennifer
et al.

Publication Date

2023-12-22

DOI

10.1126/sciadv.adj3594

Copyright Information

Peer reviewed

Single-cell analysis in hypersaline brines predicts a water-activity limit of microbial anabolic activity

Emily R. Paris[1]†, Nestor Arandia-Gorostidi[1]‡, Benjamin Klempay[2], Jeff S. Bowman[2], Alexandra Pontefract[3], Claire E. Elbon[4], Jennifer B. Glass[4], Ellery D. Ingall[4], Peter T. Doran[5], Sanjoy M. Som[6], Britney E. Schmidt[7], Anne E. Dekas[1]*

Hypersaline brines provide excellent opportunities to study extreme microbial life. Here, we investigated anabolic activity in nearly 6000 individual cells from solar saltern sites with water activities (a_w) ranging from 0.982 to 0.409 (seawater to extreme brine). Average anabolic activity decreased exponentially with a_w, with nuanced trends evident at the single-cell level: The proportion of active cells remained high (>50%) even after NaCl saturation, and subsets of cells spiked in activity as a_w decreased. Intracommunity heterogeneity in activity increased as seawater transitioned to brine, suggesting increased phenotypic heterogeneity with increased physiological stress. No microbial activity was detected in the 0.409-a_w brine (an $MgCl_2$-dominated site) despite the presence of cell-like structures. Extrapolating our data, we predict an a_w limit for detectable anabolic activity of 0.540, which is beyond the currently accepted limit of life based on cell division. This work demonstrates the utility of single-cell, metabolism-based techniques for detecting active life and expands the potential habitable space on Earth and beyond.

INTRODUCTION

Life as we know it requires liquid water. Water activity (a_w)—measured on a scale of 1 (pure water) to 0—quantifies the amount of free water molecules in an environment, making a_w a meaningful indicator of whether that environment is habitable with respect to water availability. For example, seawater has an a_w of ~0.98, most microbes cease cell division below 0.9, and fewer than 10 prokaryotic strains have been shown to continue cell division at $a_w < 0.755$ (1–4). The lowest a_w reported to sustain prokaryotic cell division in pure culture is 0.635, and extrapolations from the pure culture observations suggest a lower limit of 0.611 (1). The lowest a_w recorded for fungal germination in vitro is 0.585 (5). While it is likely that some modes of metabolic activity continue at a_w values lower than that where cell division ceases, the extent of this nonreplicative activity has not been determined. Furthermore, the a_w limit for neither detectable metabolism nor cell division has been determined in complex (environmental) halophilic communities, where it might be beyond that observed in pure cultures. Accurately identifying these limits is essential to predicting habitability on Earth and other ocean worlds and may be applied in the fields of food preservation (6), habitat management during anticipated droughts (7, 8), planetary protection (9), and selection of targets for extraterrestrial life–detection missions (10).

In addition to water activity, microbial growth can also be supported or inhibited by the specific solutes present in a cell's environment. For example, both glycerol and $MgCl_2$ lower a_w, but glycerol enhances cell growth by acting as an osmoprotectant (11–13), while $MgCl_2$ denatures biomolecules as a chaotrophic agent (14–16). In some hypersaline systems—such as seawater-sourced, salt-harvesting facilities (i.e., solar salterns)—chaotropicity, salinity, and ion concentrations all increase as a_w decreases (17), making a_w a particularly useful single metric to predict habitability in those systems.

Most previous studies investigating the a_w limits of life focused on the point at which cell division ceases [e.g., (1, 5)]. While considered a fundamental criterion for life detection (18), cell division by microbes under extreme conditions can take years to decades (11, 19), making its observation challenging and prone to underestimates. In addition, measuring cell division requires cultivation, which excludes most microbial strains from analysis. Detecting growth within complex, naturally adapted environmental communities may extend known habitability limits further by including uncultivated microorganisms that are more resilient to extreme conditions.

Environmental studies analyzing life at extremes often use the detection of various biomolecules as indicators of potentially viable microbes rather than direct measures of activity (15, 20–22). However, relic DNA (14, 17, 23–25) and adenosine triphosphate (ATP) (26), as well as cell structure (16) can be preserved in brine, leading to potential overestimation of microbial diversity, activity, and abundance when assessed by these methods. Alternatively, measuring uptake of isotope-labeled substrates in environmental samples is both tractable and definitive, directly quantifying modern anabolic activity (i.e., synthetic metabolic processes related to the growth and maintenance of biomass), in uncultured cells [e.g., (27)]. Furthermore, measuring substrate uptake at the single-cell level can lower detection limits compared to bulk analyses [e.g. (28)], making single-cell observations of substrate uptake well suited for exploring the limits of life.

[1]Department of Earth System Science, Stanford University, Stanford, CA 94305, USA. [2]Scripps Institution of Oceanography, UC San Diego, La Jolla, CA 92037, USA. [3]Johns Hopkins University Applied Physics Laboratory, Laurel, MD 20723, USA. [4]School of Earth and Atmospheric Sciences, Georgia Institute of Technology, Atlanta, GA 30332, USA. [5]Department of Geology and Geophysics, Louisiana State University, Baton Rouge, LA 70803, USA. [6]Blue Marble Space Institute of Science, Seattle, WA 98104, USA. [7]Departments of Astronomy and Earth and Atmospheric Sciences, Cornell University, Ithaca, NY 14853, USA.
*Corresponding author. Email: dekas@stanford.edu
†These authors contributed equally to this work.
‡Present address: Department of Marine Biology and Oceanography, Institut de Ciències del Mar, CSIC, Barcelona 08003, Spain.

Here, we use nanoscale secondary ion mass spectrometry (nanoSIMS) to quantify cell-specific microbial anabolic activity across a gradient of a_w within South Bay Salt Works (SBSW), a seawater-sourced solar saltern on the west coast of the United States. Our previous work at SBSW, as well as that of others, sequenced DNA and/or detected cell structures via microscopy across a range of a_w but did not detect microbial activity directly at water activities substantially below seawater (17, 29–32). In the present study, we investigate net carbon and/or nitrogen assimilation from five isotope-labeled substrates at five sites ranging from the approximate a_w of seawater to an a_w beyond the known limit of detectable cell division. We improve upon our previous study here by lowering our detection limits with increased substrate additions and by incubating cells under closer-to in situ conditions. Overall anabolic activity was observed by uptake of $^{13}C^{15}N$-amino acids or ^{15}N-ammonium—both widely assimilable by microorganisms—and specific metabolic capabilities were observed by uptake of ^{15}N-nitrate, ^{13}C-bicarbonate, and ^{13}C-glucose. We report how the magnitude and proportion of cells assimilating these substrates, the intracommunity heterogeneity in activity, and the relative use efficiency (RUE) of carbon versus nitrogen from amino acids changes along the gradient of a_w. Last, we extrapolate our results to estimate a lower a_w limit of detectable anabolic activity.

RESULTS

Brine geochemistry

We recorded physical and geochemical characteristics (tables S1 to S3) of five sites at SBSW (fig. S1), which are numbered here in order of decreasing a_w: site I (a seawater conduit), sites II, III, and IV (NaCl-dominated brines), and site V (an MgCl$_2$-dominated brine) (Table 1). For previously published site names of sites IV and V, see table S1. The in situ pH of sites I to III were slightly basic (~8), while the pH of site V dropped to ~5. Ratios of Mg^{2+}/Na^+, a proxy for chaotropicity (17), ranged from 0.15 to 0.32 in sites I to IV and increased to 44.67 in site V. Organic and inorganic compounds and microbial cell density generally increased as a_w

decreased throughout the system (tables S3 and S4). Since a_w is temperature dependent, we measured the a_w values of brines in the field at ambient temperature (table S1) as well as in our incubation bottles at incubation temperature (33°C) (Table 1). We use the latter values in all further analyses/discussion. We modeled the a_w of evaporating seawater at NaCl saturation to be 0.742 at 33°C, indicating that site IV (measured a_w = 0.717) had reached saturation (a "crystallizer" pond).

Microbial community composition

Microbial community composition was determined at each site (fig. S2). The communities reflected typical taxonomy for seawater-sourced solar salterns and, specifically, that measured previously at SBSW (17, 32, 33). Site I was dominated by Alphaproteobacteria, with *Candidatus* Pelagibacter as the most relatively abundant taxon. Each site between sites II and V had a unique prokaryotic community composition (analysis of similarities: $R = 1$, $P < 0.001$) with taxonomic overlap between sites, indicating a continuous microbial community succession from NaCl brines (sites II to IV) to the MgCl$_2$ brine (site V) [consistent with (17)]. Site II was dominated by *Psychroflexus*, *Spiribacter*, and *Halolamina*. The most relatively abundant taxon in site III was *Halobonum*, but the two amplicon sequence variants (ASVs) associated with this taxon were not highly abundant in other sites. *Salinibacter ruber* was the most relatively abundant bacterial taxon in sites III to V, peaking in relative abundance in site IV. Archaea, specifically Halobacteria, were more abundant than bacteria overall in sites III to V, which experienced a shift from *Halobonum* dominating site III to *Haloquadratum walsbyi* dominating sites IV and V.

Single-cell substrate assimilation

Water activities at 33°C (the incubation temperature) of the incubations ranged from 0.982 ± 0.001 in site I to 0.409 ± 0.012 in site V (Table 1). After a 48-hour incubation time, 1832 putative cells [regions of interest (ROIs)] were analyzed with nanoSIMS for $^{13}C^{15}N$–amino acid uptake, 973 ROIs for ^{13}C-bicarbonate and ^{15}N-ammonium uptake, and 1049 ROIs for ^{15}N-nitrate and ^{13}C-glucose uptake. These were compared to isotope values at the initial time point of 768, 760, and 506 ROIs from each substrate combination, respectively, to determine isotope enrichment. Isotope information for all ROIs is included in dataset S1. Our average net assimilation minimum detection limits (C_{net}% and N_{net}%) ranged from 0.55 to 3.11% and 0.33 to 1.36%, respectively (table S5), which makes our analysis up to two orders of magnitude more sensitive than measuring cell division (the theoretical C_{net}% and N_{net}% of each daughter cell is ~50%).

Average total anabolic activity, measured by uptake of amino acids and ammonium, decreased exponentially with a_w (Fig. 1A, insets). However, subsets of cells in site II were more active in assimilation of carbon from amino acids (9 of 355 cells analyzed), nitrogen from ammonium (10 of 137 cells analyzed), and carbon from glucose (24 of 222 cells analyzed) than the most enriched cells in site I. The proportion of active cells remained relatively high in sites I to IV despite decreasing net assimilation values at lower a_w (Fig. 1). Two cells (of 290 analyzed) were slightly above the ^{13}C-amino acids and ^{13}C-glucose enrichment thresholds in site V, the only MgCl$_2$-dominated brine (C_{net}% for amino acids = 0.37% and C_{net}% for glucose = 5.90%; detection limits = 0.35 and 5.87%,

Table 1. Overview of sampled sites. Sites sampled, dominant salt type, and key environmental parameters known to affect habitability in brines: average water activities ± SDs of triplicate measurements from the incubations derived from these sites (measured at 33°C, the incubation temperature), ionic strength, the ratio of Mg^{2+} to Na^+ (a proxy for chaotropicity), and salinity as total dissolved solids (TDS).

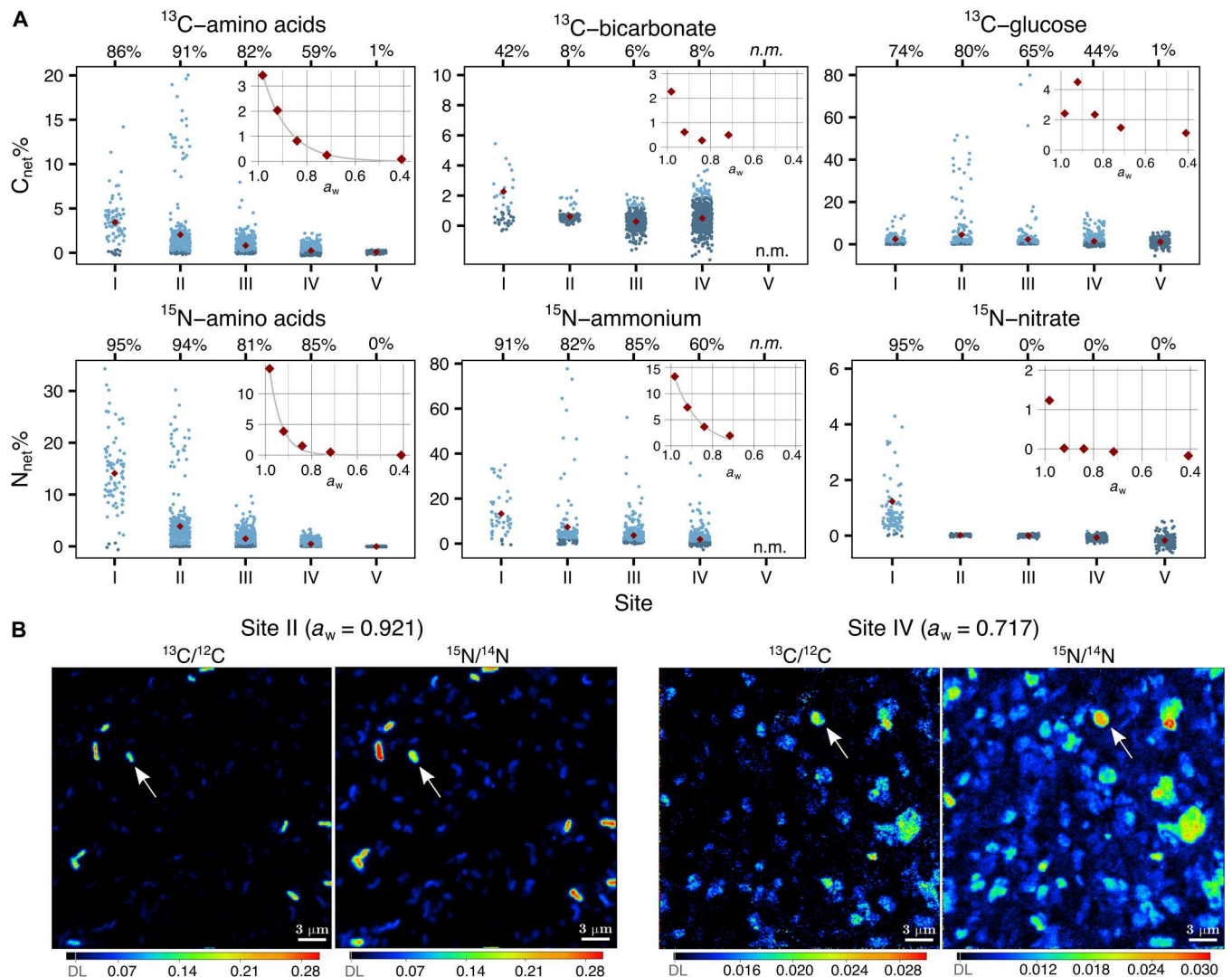| Site	Dominant salt type	a_w (33°C)	Ionic strength (M)	Mg^{2+}/Na^+ (M)	TDS (g/liter)
I	NaCl	0.982 ± 0.001	0.714	0.15	39
II	NaCl	0.921 ± 0.004	3.025	0.29	151
III	NaCl	0.840 ± 0.001	5.270	0.28	248
IV	NaCl	0.717 ± 0.001	6.923	0.32	337
V	MgCl$_2$	0.409 ± 0.012	12.642	44.67	350

Fig. 1. Single-cell incorporation of six isotope labels across the sampled a_w gradient. (**A**) Net assimilation of carbon (C_{net}%, top row) and nitrogen (N_{net}%, bottom row) for each site, arranged in order of decreasing a_w (I, 0.982; II, 0.921; III, 0.840; IV, 0.717; V, 0.409). Substrate combinations within the same incubation bottle are stacked (i.e., ^{13}C-bicarbonate and ^{15}N-ammonium). Light and dark blue points are cells with net assimilation values above and below the detection limit for substrate assimilation, respectively. The proportions of cells with detectable substrate uptake (rounded to the nearest whole number) are above the plot for each site. Red diamonds indicate average net assimilation of active and inactive cells (replotted in insets with the same y-axes units as the main plots). Insets of general activity substrates include exponential curves (gray) that were fit using a nonlinear least squares regression model, and fits were assessed with root mean squared error (RMSE): ^{13}C-amino acids, 0.063; ^{15}N-amino acids, 0.366; ^{15}N-ammonium, 0.378. Two points are not displayed for enhanced visualization: (1) site I [$C_{net(bicarbonate)}$% = 48.8%] and (2) site I [$N_{net(nitrate)}$% = 33.9%]. n.m., not measured. (**B**) NanoSIMS isotope ratio images of cells incubated with $^{13}C^{15}N$-amino acids in site II (left) and site IV (right). Color bars begin at natural abundance (0.011 for $^{13}C/^{12}C$ and 0.0037 for $^{15}N/^{14}N$) and are scaled variably by image. Detection limits (DL) were added manually to the color bars (gray solid lines). From left to right: Detection limits in ratio form are 0.012, 0.006, 0.011, and 0.004. White arrows point to examples of individual cells enriched in both ^{13}C and ^{15}N. See fig. S6 for more nanoSIMS images.

respectively). However, this unlikely reflects true activity (see Discussion).

Assimilation of bicarbonate and nitrate was relatively low in sites II to IV, in both proportion of cells assimilating the substrates and the quantity assimilated by those cells (Fig. 1A). We compared the uptake of bicarbonate to that from ammonium in individual cells to determine the fraction of total cellular carbon derived from inorganic carbon per cell and, therefore, autotrophy versus heterotrophy, as in (*34*) (fig. S3). This revealed that although 42% of the community had incorporated some bicarbonate in site I, only 2%

of the community derived more than 50% of its newly assimilated cellular carbon from bicarbonate. This indicates that most cells assimilating bicarbonate in site I were likely heterotrophic or potentially mixotrophic. However, 79% of the cells with detectable bicarbonate assimilation in site IV (6% of the total community) derived greater than 50% of their new cellular carbon from bicarbonate, indicating that they were likely autotrophs. Last, while most cells (95%) assimilated nitrate in site I, no cells were found to be enriched in ^{15}N from nitrate in sites II to V.

C:N RUE

C:N RUE describes the amount of C relative to N incorporated into a single cell from uptake of $^{13}C^{15}N$-amino acids (*35*). Here, average C:N RUE increased as a_w decreased, with individual cell values ranging from approximately 0.1 to 2.9 (Fig. 2). Stochiometric incorporation (i.e., C:N RUE = 1.0) of carbon and nitrogen was achieved by some cells in sites II to IV, and the highest C:N RUE values were found in site IV.

Intracommunity activity distribution and taxonomic richness

We used the Gini coefficient (*36*) to quantify unevenness in the distribution of anabolic activity within a microbial community as in (*28*). Gini coefficients closer to 1 indicate a more heterogeneous, or uneven, distribution of anabolic activity (i.e., fewer cells are responsible for more substrate uptake). All three indicators of general anabolic activity used here—uptake of carbon and nitrogen from amino acids and uptake of nitrogen from ammonium—show that intracommunity heterogeneity in single-cell uptake jumps during the transition from seawater to brine (between sites I and II). However, all three substrates also indicate that heterogeneity does not continue to increase consistently with further decreasing a_w, as the Gini coefficient decreased slightly between sites II and III and then increased again in site IV (Fig. 3A). To better understand the trends presented by the Gini coefficient, we compared ASV-level taxonomic richness (Fig. 3, B and C) and unevenness (fig. S4) to intracommunity activity heterogeneity. Linear regression suggests a strong relationship between activity heterogeneity and taxonomic richness ($R^2 = 0.997$, $P = 0.001$) but no correlation to taxonomic unevenness (fig. S4B; $R^2 = 0.055$, $P = 0.767$).
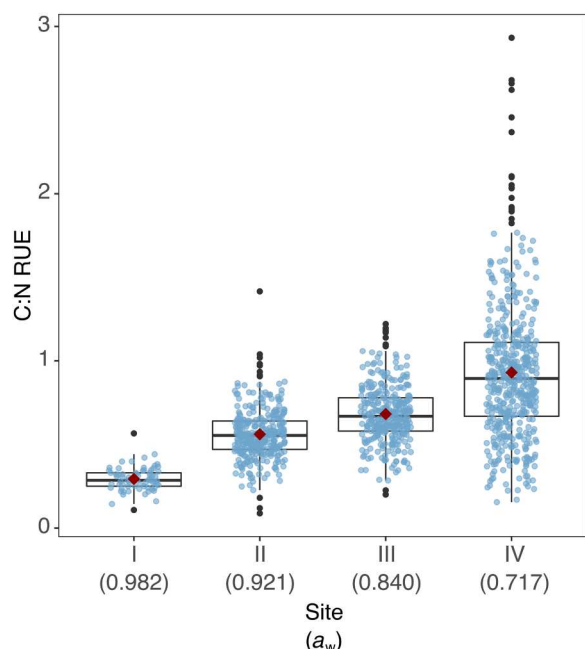

Fig. 2. C:N RUE from uptake of $^{13}C^{15}N$-amino acids. Sites are ordered by decreasing a_w (I, 0.982; II, 0.921; III, 0.840; IV, 0.717). Site V is not included because no activity was detected in uptake of ^{15}N-amino acids. Box plots include outliers (black points), upper (75th percentile) and lower (25th percentile) quartiles, and median. Red diamonds represent means.

Estimating the a_w limits of detectable anabolic activity

We used the average net assimilation values of active cells in each site to estimate a_w limits of detectable anabolic activity in natural brine communities (Fig. 4). Linear regression of the log-transformed average net assimilation values of ^{13}C-amino acids from each site predicted a minimum a_w of 0.540, with upper and lower 95% confidence interval bounds of $a_w = 0.662$ and 0.418, respectively ($R^2 = 0.99$, $P = 0.01$). That for ^{15}N-amino acids and ^{15}N-ammonium were higher, at 0.583 (bounds of $a_w = 0.751$ and 0.416; $R^2 = 0.97$, $P = 0.02$) and 0.568 (bounds of $a_w = 0.858$ and 0.279; $R^2 = 0.91$, $P = 0.04$), respectively. Using the reaction-path modeling code EQ3/6 (*37*), we calculated the total Mg^{2+} concentration and ionic strength of a 0.540-a_w brine in this saltern system to be approximately 3.58 and 11.44 M (fig. S5), respectively.

DISCUSSION

Low-a_w environments—from the ocean to hypersaline brines—are abundant on Earth (*38*, *39*). They are also key features of numerous potential habitats on other planets and icy moons due to their depressed freezing point (*40*, *41*). In addition, as droughts become more common on Earth because of climate change, some microbial communities will encounter lower a_w than usual, which will affect ecosystems on micro and macro levels (*7*, *8*). Low a_w can influence microbial habitability by limiting enzyme function, damaging cellular structure, and causing osmotic stress (*16*, *42*–*44*). While pure culture studies have advanced our knowledge of the a_w limits of cell division (*1*, *5*, *11*, *14*, *15*, *45*, *46*), measurements of microbial activity in complex environmental brines are rare. Understanding how a_w influences microbial metabolism will advance knowledge of adaptation and community function in brines, help predict responses of modern communities to future shifts in salinity, and inform the search for life on other planets.

Here, we measured microbial assimilation of carbon and nitrogen from a suite of substrates to directly quantify anabolic activity in low-a_w brines. At the community level, our data showed that as a_w decreased, average net assimilation of amino acids and ammonium (proxies for total anabolic activity) decreased exponentially (Fig. 1). This is consistent with and expands upon previous community-level observations including work that measured a decrease in bulk assimilation of [^3H]leucine, sulfate reduction rates, and methanogenesis rates with increasing salinity in different solar salterns (*27*, *47*). However, our single-cell results also revealed several findings obscured by bulk analysis. For instance, subsets of cells (3 to 11%) were more anabolically active with a moderate decrease in a_w, and the majority of the natural community (up to 85% of cells) remained active even as the brine surpassed the a_w of NaCl saturation (0.742 at 33°C) in site IV. As a_w dropped from 0.982 in site I to 0.717 in site IV, the proportion of cells actively assimilating nitrogen from amino acids decreased by only 11%, while average net assimilation decreased by 97%. These trends are likely due to a combination of shifts in community composition and physiological responses within taxa as conditions change. The spike in highly active cells between seawater and brine may reflect the rise of taxa adapted to lower a_w (e.g., *Spiribacter* and *Halolamina*, fig. S2), which are invigorated by more suitable conditions and potentially by decreasing competition as other lineages cease activity. Alternatively, spikes in anabolic activity may reflect increased turnover of biomolecules and/or cellular repair processes as cells not adapted to lower a_w
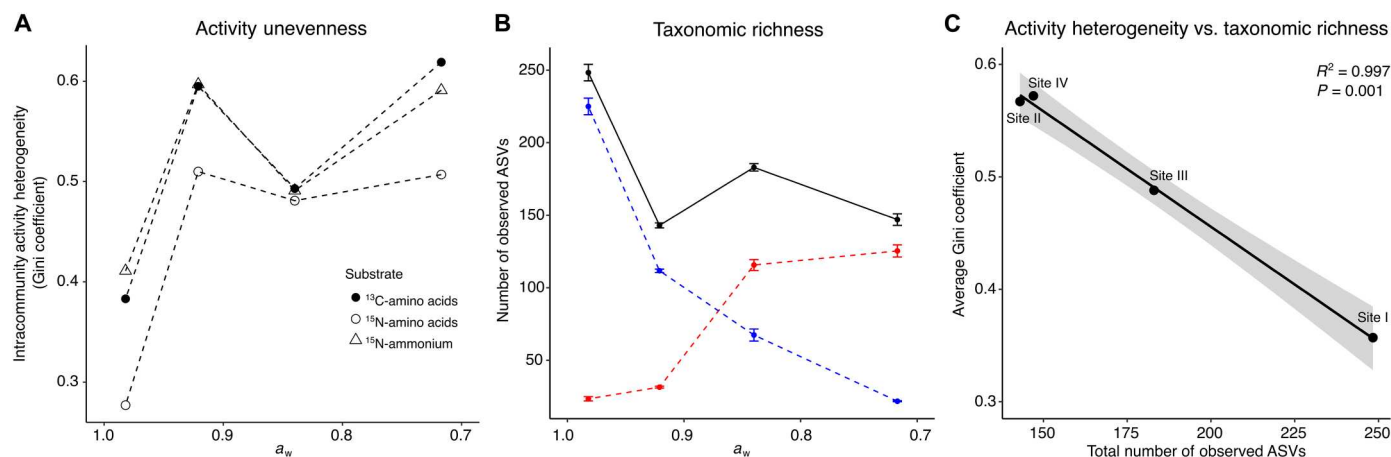
Fig. 3. Intracommunity activity heterogeneity (Gini coefficient) and taxonomic richness with decreasing a_w. (**A**) Activity heterogeneity is lowest at high a_w for uptake of ^{13}C-amino acids, ^{15}N-amino acids, and ^{15}N-ammonium measured by nanoSIMS. (**B**) Taxonomic richness is highest at high a_w and is represented as averages of total ASVs (black), bacterial ASVs (blue), and archaeal ASVs (red) from 10,000 randomly subsampled 16S ribosomal RNA gene reads per site. Error bars represent SEs of triplicate DNA collections. (**C**) Relationship between intracommunity activity heterogeneity (average of Gini coefficients for uptake of ^{13}C and ^{15}N from amino acids and ^{15}N from ammonium) and taxonomic richness (total observed ASVs) ($R^2 = 0.997$, $P = 0.001$). Shaded area represents the 95% confidence interval.

attempt to maintain viability. Meanwhile, the overall decrease in activity across the gradient likely reflects increasingly slow growth rates of even highly adapted halophiles, such as *Haloquadratum* (*1*), as NaCl saturation is approached and surpassed. In addition to decreasing a_w, cell activity may have been hindered by other environmental stressors that increase with evapoconcentration, including increasingly recalcitrant carbon (unavailable for cellular use), ionic strength, acidification, chaotropicity (tendency for molecules to disrupt hydrogen bonding), and high metal concentrations (*14, 17, 45, 48, 49*).

Activity trends with decreasing a_w were more variable for nitrate, glucose, and bicarbonate, likely because they are metabolism-specific substrates and do not reflect activity across all organisms. Nitrate uptake was only detected in site I, which may be explained by inhibition of nitrate reductase by high in situ ammonium concentrations (*50*) in sites II to V. Nitrate reductase could also be inhibited by increasing concentrations of Mg^{2+} or other heavy metals (*51, 52*). Uptake of glucose peaked in site II, potentially because of increased demand for precursors of osmolytes. Osmolytes, like trehalose, are used by a wide variety of halotolerant and halophilic organisms to combat salt stress (*53*). However, glucose uptake calculations are approximate because of limitations in estimating in situ glucose concentrations (see Materials and Methods). Bicarbonate uptake was low across the sample set, and comparison to single-cell, ammonium-based growth rates indicated that the bicarbonate uptake observed was primarily due to heterotrophic fixation of inorganic carbon rather than autotrophy. Fixation of inorganic carbon by heterotrophs can occur via multiple metabolic processes, e.g., anaplerotic reactions, and contributes a considerable amount to total carbon fixation in diverse environments (*54*). While photoautotrophic eukaryotes, particularly *Dunaliella salina*, are typically considered the main endogenous sources of organic carbon in high-salinity brines (*55*), our data indicate that fixation of inorganic carbon by heterotrophs also contributes, even at NaCl saturation.

Cells in site V (the only MgCl$_2$-dominated site) were not found to have significant anabolic activity despite the presence of biomass-

like material identified by nanoSIMS and 4′,6-diamidino-2-phenyl-indole (DAPI) staining (figs. S6 and S7). Two cells in this site were slightly above the detection limits for enrichment: one after incubation with ^{13}C-amino acids and one after incubation with ^{13}C-glucose. However, given the probabilistic nature of our thresholds for significant enrichment, we would expect 0.1% false positives and, therefore, do not consider the detection of only two slightly enriched cells a robust indication that activity occurred in that brine. Site V had a high concentration of Mg^{2+} ions (~4 M), and the concentration prohibitive to life is expected to be lower (~2 to 3 M) (*14, 15*). Ionic strength in site V (12.642 M) was also slightly higher than the currently accepted ionic strength permissible to growth (12.141 M) (*56*). Furthermore, combined low a_w and pH can affect microbial growth [e.g., (*57, 58*)], and site V was the most acidic brine of the five sampled sites. Therefore, cells in site V were likely inhibited by multiple stressors. Future single-cell investigations of microbial metabolism in chaotropic and/or acidic brines with a_w below 0.7 could disentangle these various effects.

We observed that the RUE for carbon relative to nitrogen increased with decreasing water activity (Fig. 2). The C:N RUE values are generally lower than expected in coastal ecosystems (*35*), potentially because of dilution of assimilated ^{13}C by natural-abundance carbon in the polycarbonate filters during analysis (*59*). However, the upward trend in RUE with decreasing a_w remains robust. Greater demand for carbon relative to nitrogen from amino acids by some cells may reflect processes associated with salt adaptation. Cells can accumulate amino acids (via uptake or synthesis) and other organic compounds (i.e., osmolytes) to prevent cellular water loss from osmotic stress in hypersaline environments (*53, 60*). Thus, the inverse relationship between C:N RUE and a_w may be related to osmolyte synthesis as water stress increases. In addition, some halophiles (including *H. walsbyi* and *S. ruber* detected here) have more acidic proteomes and cell walls than other microbes to combat ionic imbalance caused by salt-in adaptation mechanisms (*61*). This is accomplished by using amino acids like glutamate and aspartate, which have high C:N ratios compared to less acidic amino acids (*2, 62*). Given that incorporation of more
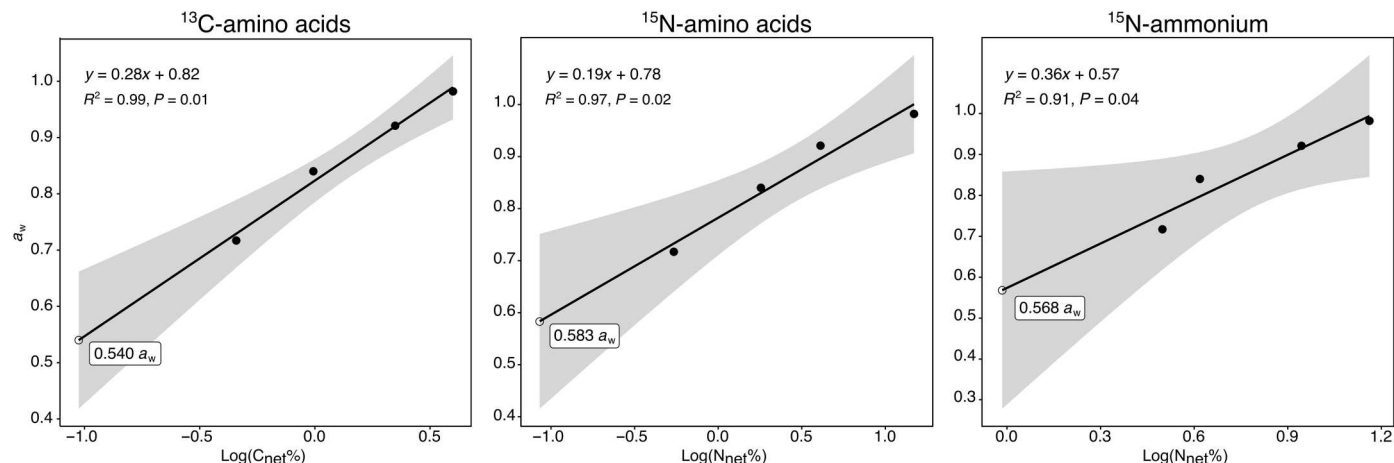
Fig. 4. Estimated a_w limits for detectable anabolic activity using linear regression. Closed circles represent average $\log(C_{net}\%)$ or $\log(N_{net}\%)$ values for active cells in each lake. Open circles represent estimated a_w limits (value in box) for detectable anabolic activity. Shaded area represents 95% confidence intervals.

acidic amino acids and accumulation of osmolytes may increase the C:N RUE value of a cell, higher C:N RUE values at lower a_w could reflect the presence of more active halophiles in a hypersaline environment.

We found that intracommunity heterogeneity in activity increased (i.e., fewer cells contributed to more of the detected anabolic activity) when a_w decreased below that of seawater. This trend occurred as taxonomic richness decreased, indicating that the increase in activity heterogeneity was not driven by increasing genomic diversity. Recent data have suggested that phenotypic heterogeneity (e.g., variable rates of anabolic processes within genetically identical populations) increases with nutrient limitation and/or physiological stress (63, 64). Although rarely measured in complex environmental samples, our previous work suggests that metabolic heterogeneity indeed increases with physical and nutritional stress as water depth increases in the ocean (28). Here, an underlying combination of increasingly stressful environmental parameters may have contributed to both decreasing taxonomic richness and increasing heterogeneity in activity. Therefore, the inverse relationship between metabolic heterogeneity and taxonomic richness could be explained by greater phenotypic heterogeneity within individual populations.

Establishing the limit of life at low a_w is important for understanding fundamental biology on Earth and is required for planning life detection missions to other worlds. We hypothesized that the a_w limit of life based on anabolic activity was beyond previous estimates that were based on observations of cell division in pure cultures. Although cell division is ultimately required for a microbial community to grow and evolve, using direct observations of cell division as an indicator of habitability is likely to lead to underestimates due to the technical challenges of the observation, including time. Observing substrate assimilation has the advantage of detectability long before division occurs, although this comes with the arguable disadvantage of including activity related to repair/maintenance of biomass in addition to growth. However, even if the assimilation detected is related to nonreplicative activity, it indicates that the cells are currently viable and, therefore, of interest from the perspective of habitability, planetary protection, and food preservation. By observing substrate assimilation with nano-SIMS, we were able to detect anabolic activity two orders of

magnitude less than required for cell division, and, by using naturally adapted halophilic communities, we increased the likelihood of including uncultured and potentially more resistant strains. Furthermore, single-cell analysis allowed us to exclude inactive cells from our dataset when projecting the a_w limit, which otherwise might have been skewed by biomass not endemic to the brine (deposited by, e.g., wind).

With this approach, we estimated a lower theoretical limit of detectable activity at $a_w = 0.540$. This a_w exceeds the measured (0.635) and modeled (0.611) a_w limits of cell division for halophilic prokaryotes in culture (1) as well as the current measured (0.585) and modeled (0.565) a_w minima for fungal germination (5). Microbial life is sensitive to even small changes (± 0.010) in a_w (65). Thus, the difference between the previous and newly proposed limits is physiologically notable and suggests a larger potential habitable space for anabolically active life. Furthermore, it is possible that the true limit of anabolic activity is lower than our estimate, both for technical reasons (e.g., our estimate is limited by the detection limit of our assay) and biological reasons (e.g., there may be more resilient microorganisms in other environments, and the compounding chemical stressors along the a_w gradient in this saltern system may have decreased viability faster than a_w would have alone).

In addition to a_w, understanding the ionic composition of an environment is fundamental in determining its overall habitability. Even when a_w is permissible to life, other factors—such as ionic strength and chaotropicity—can impose additional stressors that may affect cell division [e.g., (14, 15, 56, 66–68)]. According to our model results, a seawater-sourced brine with an a_w of 0.540 is consistent with an ionic strength of ~11.4 M and a total aqueous Mg^{2+} concentration of ~3.6 M. Our predicted ionic strength is below the measured limit of ionic strength (~12.1 M) but slightly above existing dissolved $MgCl_2$ concentration limits [~2 to 3 M; (14, 15, 56, 69)]. Given current knowledge, this suggests that life would be limited by high Mg^{2+} concentrations before low a_w in this system. However, the presence of kosmotropic (biomolecule-stabilizing) agents in a natural environment may increase tolerance to Mg^{2+} (14), including glycerol released by *Dunaliella* (13). Further work is needed to understand how high Mg^{2+} affects metabolic

activity in situ. It is also important to acknowledge that the a_w limit of detectable activity may be higher than 0.540 in polyextreme environments, such as high-pressure chaotropic brines on the seafloor (14, 15, 39), magnesium sulfate–dominated environments on Earth [e.g. (56, 68)], and regions of Mars with high ionic strength (45).

In conclusion, our work indicates that anabolic activity likely continues beyond the previously established water activity (a_w) limit for cell division and suggests 0.540 as a minimum a_w for detectable anabolic activity in seawater-sourced brines. This has implications for life detection in environments on Earth and other worlds with areas of low a_w, such as putative liquid flows on Mars (70) and brines within moons like Europa (71, 72), Titan (73), and Enceladus (74). Together, our data demonstrate the power of single-cell analysis when working at the limits of detectable metabolism and provide a methodology for future research into the limits of life in extreme environments.

MATERIALS AND METHODS

Experimental design
The objective of this study was to measure microbial anabolism in environmental samples across a water activity gradient. Sampling was conducted with sterile tubing and a peristaltic pump at multiple sites ranging from 0.982 to 0.409 a_w. Geochemical analysis was conducted to contextualize activity measurements. Two-day incubations with combinations of five different stable isotope–labeled substrates were started within 24 hours of sampling, and single-cell isotope analysis quantified substrate uptake in nearly 6000 individual cells. Specific sampling and experimental details are described below.

Sample collection and geochemical analysis
Brine was sampled in October 2020 from five sites at SBSW in Chula Vista, California, USA (32.6°N, 117.1°W; fig. S1); see (17) for site details. Briefly, seawater enters the facility through a conduit (site I) and is moved through a series of open-air ponds (e.g., sites II to V), where it evaporates under natural conditions until NaCl and subsequently MgCl$_2$ reach saturation, precipitate out, and are harvested for commercial purposes. In situ temperature and pH were measured at each site with the Onset HOBO MX2501 pH and temperature logger, and in situ a_w was measured with the AQUALAB 4TE dew point water activity meter (instrument error was ±0.003) (table S1).

Brine was collected and stored at ambient temperature, and filtration (0.2 μm) for geochemical analyses was performed upon return to the laboratory. Amino acid concentrations were measured with a fluorometric method designed for seawater samples (75), and nitrate and ammonium concentrations were determined with spectrophotometry (76, 77). Dissolved organic carbon concentrations were measured as nonpurgeable organic carbon using high-temperature catalytic oxidation with a Shimadzu TOC-VCSN analyzer (78, 79). Total dissolved solids were measured by ACZ Laboratories Inc. (Steamboat Springs, CO, USA) from residues of evaporated samples. Ions and metal concentrations were quantified at ACZ Laboratories with gravimetric ion chromatography (bromide, fluoride, and chloride only), automated colorimetric (phosphorus only), and inductively coupled plasma (metals and all other reported ions). The ratio of Mg^{2+} to Na$^+$ was calculated as a proxy for chaotropicity as in (17). Ionic strength was calculated as in (45).

Brine samples for stable isotope incubations were collected unfiltered in 2-liter, acid-washed polycarbonate bottles using a peristaltic pump and returned to the laboratory within 12 hours. One bottle was collected per site. The a_w of NaCl saturation at 33°C was estimated by modeling the evaporation of seawater as in (17) and recording the a_w of halite at NaCl precipitation.

16S ribosomal RNA gene extraction, sequencing, and analysis
Cells from 4 to 100 ml of brine from each sampling site (depending on the viscosity and filter capacity) were vacuum filtered onto sterile 0.2-μm Supor filters (47 mm; PALL) on site and stored on dry ice. DNA was extracted with the MagMax Microbiome Ultra kit (Thermo Fisher Scientific) on a KingFisher Flex bead-handling robot and quantified with a Qubit 3.0. 16S ribosomal RNA (rRNA) amplicon library construction and sequencing were completed at the Argonne National Laboratory (Lemont, IL, USA) with 515F/806R universal prokaryotic primers (80), and amplicon libraries were sequenced with the Illumina MiSeq platform (2 × 151 paired-end reads) (BioProject: PRJNA680352). Reads were processed with dada2 (81) and paprica (v0.7.0) (82) as described in (17). Alpha diversity metrics were calculated by randomly subsampling to 10,000 reads.

Stable isotope incubations
One hundred milliliters of brine from each site was incubated in duplicate with three separate stable isotope combinations: (i) 500 μM ^{13}C-bicarbonate (Cambridge Isotopes CLM-441) and 2 μM ^{15}N-ammonium chloride (NLM-467), (ii) 2 μM ^{13}C-glucose (CLM-1396) and 2 μM ^{15}N-sodium nitrate (NLM-157), and (iii) 2 μM ^{13}C^{15}N-algal amino acid mixture (CNLM-452). Concentrations of isotope-labeled substrates were selected to be higher here than in a previous experiment conducted at this site (17) to lower detection limits. Incubation conditions were also chosen to reflect in situ conditions more closely, additionally increasing the likelihood of detecting activity. Static incubations were conducted in an environmental chamber at 33°C with light (350 to 500 μmol/m^2 s) for 12 hours per day. Immediately after isotope addition (T$_i$) and after 48 hours (T$_f$), incubations were harvested. Forty-eight hours was selected as the final time point to maximize assay sensitivity and therefore the ability to observe low levels of activity in these slow-growing communities; previous work in this system indicated no significant community shifts during 48 hours of bottle incubation (17). Whole incubations were fixed with 4% paraformaldehyde for 1 hour at room temperature and filtered onto sterile 0.2-μm polycarbonate filters (25-mm diameter) using a vacuum pump. Water activity was measured in triplicate from unfixed incubation filtrate (0.2 μm) after isotopic substrate addition at the incubation temperature (33°C) (Table 1). Filters were washed once with 10% phosphate-buffered saline (PBS) and twice with Milli-Q water to remove salts. Cells were dehydrated by soaking the filters in PBS: EtOH (50:50) and 100% EtOH for 2 min each. Then, filters were stored at −80°C until further analysis.

DAPI imaging
To investigate the possible presence of intact cells in site V, ^{13}C^{15}N-amino acid incubation filters were imaged with DAPI-based Vectashield (no. H-1200, Vector Laboratories Inc., Burlingame, CA,

USA) using a Nikon ECLIPSE Ti2 microscope with a 100× oil immersion lens.

NanoSIMS imaging

Single-cell uptake of carbon and nitrogen was analyzed via nanoSIMS. Sections of the T_i and T_f filters (from one of the two replicate incubations) were mounted onto conductive carbon tabs and sputter coated with 20 nm of gold. Areas of the filter were randomly selected and analyzed by the NanoSIMS 50 L (CAMECA, Gennevilliers, France) housed in the Stanford Nano Facility using a Cs^+ primary beam operating in continuous mode. The beam was set at 4 pA with an approximately 100-nm spot at the sample surface. Samples were analyzed using a 256 × 256 pixel raster on 30 µm by 30 µm areas with a dwell time of ~1 ms per pixel. Presputtering with a high-energy beam was conducted for 30 s. The following masses were collected with electron multipliers: $^{12}C^-$, $^{13}C^-$, $^{12}C^{13}C^-$, $^{12}C_2^-$, $^{12}C^{14}N^-$, $^{12}C^{15}N^-$, and $^{32}S^-$. Thirty serial secondary ion images (i.e., layers) were collected. The mass resolving power was ~7000 [after ×1.5 correction, (83)] using an exit slit width of 70 µm, an entrance slit width of 20 µm, an aperture slit of 200 µm, and an energy slit filtering about 30% of secondary ions from the high-energy tail of their energy distribution. ROIs were hand drawn around putative cells using CN^- nanoSIMS images and LANS software (84). Between 300 and 2000 cells were analyzed per site (table S4). Cell density at each site was estimated using the number of ROIs circled on T_0 frames of view for each site and calculated to represent the number of cells per milliliter of brine.

Activity calculations

Nitrogen and carbon isotope ratios were calculated using the CN^- and C_2^- ions, respectively. ROIs with low ion counts (Poisson error values above 0.1) were removed from the dataset before further analysis. Cells were classified as enriched in ^{13}C and/or ^{15}N if the atom fraction, a, of the cell at the final time point, T_f, was above the detection limit of enrichment (DL), conservatively defined according to (34) as

$$DL_{15N} = \overline{a}_{15N,i} + (SD_{\overline{a}_{15N,i}} \times 3) \quad (1)$$

where a is the atom fraction of the minor isotope

$$a_{15N} = \frac{^{15}N}{\left(^{14}N + ^{15}N\right)} \quad (2)$$

$\overline{a}_i$ is the mean atom fraction of cells at T_i (before incubation), and $SD_{\overline{a}_i}$ is the SD of that mean. Detection limits are listed in table S5. The a_f of each cell was converted to net substrate assimilation [$X_{net(y)}$%] where X is carbon (C) or nitrogen (N) from a given substrate (y), as defined in (34). For example, $N_{net(ammonium)}$% quantifies the amount of biomass generated with ammonium during the incubation period relative to the total final biomass and is represented by

$$N_{net(ammonium)}\% = \left[\frac{(a_{15N,f} - a_{15N,i})}{(a_{15N,sub} - a_{15N,i})}\right] \times 100 \quad (3)$$

In Eq. 3, a_{sub} is the atom fraction of the isotopically spiked substrate pool, determined by proportionally averaging the atom fraction of the added isotopically labeled substrate (provided by the manufacturer) and the in situ pool of that substrate [assumed to be natural abundance, i.e., 0.0037 for a_{15N} and 0.011 for a_{13C}

based on (85)]. The a_{sub} values are reported in table S6. The average atom fraction of cells at T_i ($\overline{a}_i$) was used to approximate a_i. Site V $C_{net(glucose)}$% was calculated using the $\overline{a}_i$ values of cells from site V ^{13}C-amino acids due to a technical error with the $\overline{a}_i$ values for glucose from that site. Since in situ ammonium concentrations were below the detection limit (29 µM) in sites I and II, a_{sub} was calculated using approximated values 2 and 26 µM, respectively. These values were estimated using previously published values (86) and the linear correlation of ammonium to amino acids in this dataset ($R^2 = 0.96$, $P = 0.02$), as both substrates were assumed to follow the same trends with evapoconcentration. In situ glucose concentrations were estimated using the ratio of glucose to dissolved organic carbon in surface seawater (0.02) (87, 88).

C:N RUE values were calculated as in (35). We used a C:N value for amino acids of 4.9, which was the proportional average of the C:N ratios in each amino acid in the isotope mix (table S7). The C:N biomass ratio of hypersaline brine microbes has not yet been quantified, so the average C:N biomass ratio of coastal marine microbes (5.9) was used (89). Bias-corrected Gini coefficients were calculated using the "Gini" function in the R package "DescTools" (version 0.99.49) (90).

The proportion of autotrophic cells within the community was determined by analyzing the ratio of $N_{net(ammonium)}$% to $C_{net(bicarbonate)}$% in individual cells, as in (34) and subsequently defined as C_{diet}% in (91). Cells with $N_{net(ammonium)}$%:$C_{net(bicarbonate)}$% ratios greater than two were considered primarily heterotrophic (i.e., sourced at least 50% of their new cell biomass from organic carbon). ROIs with ratios less than 2 were considered primarily autotrophic (i.e., sourced at least 50% of new cell biomass from inorganic carbon).

Estimating the a_w limit of detectable anabolic activity

Linear regression was performed on log-transformed $C_{net(amino\ acid)}$%, $N_{net(amino\ acid)}$%, and $N_{net(ammonium)}$% data for active cells only in sites I to IV to estimate an a_w limit for detectable anabolic activity as performed previously to determine the limit for cell division in pure cultures (1). The site IV detection limits were used to calculate net assimilation values below which activity would be undetected. Then, this estimate was log transformed and used as x in the equation produced by linear regression to estimate the a_w values (y) where no detectable anabolic activity would be expected to occur.

Geochemical modeling

Simulating geochemical changes of seawater undergoing evaporation was done using the EQ3/6 code, version 8.0a. Our simulations used the generic seawater file swmajp.3i included in the distribution. Evaporation was simulated by subjecting the seawater to a negative titration by removing a total of 55.25 mol of water over the course of the reaction. The thermodynamic database used was the "ypf" database of pitzer activity coefficients. Simulations were performed at 30°C and 33°C. The water density model of EQ3/6, used to convert molalities (EQ3/6 default) to molarities (reported here), is valid between 20° and 30°C. As a result, the evaporation simulation at 33°C was used to compute the a_w of seawater at NaCl saturation, whereas the simulation at 30°C was used to compute the ionic strength and Mg^{2+} concentration at an a_w of 0.540. Electrical balancing was done on Cl^-. To bracket the solution—and because natural seawater is slightly supersaturated with respect to carbonates

—two end-member simulations were performed: one where carbonate minerals were allowed to precipitate and were maintained in thermodynamic equilibrium with the aqueous fluid, and another where their formation was suppressed. Suppressed carbonates were aragonite, artinite, calcite, dolomite, huntite, hydromagnesite, lansfordite, magnesite, and nesquehonite.

Statistical analysis

Means and SDs are reported in figures and tables where applicable. Limits of detection for uptake of carbon and nitrogen from amino acids, bicarbonate, ammonium, glucose, and nitrate are listed in table S5. Differences in ASV relative abundances (Bray-Curtis dissimilarity) between sites and within sites (replicates) were assessed with analysis of similarities (92). Regression models were assessed with coefficients of determination and P values. All data were visualized with ggplot2 in RStudio (93).

Supplementary Materials

This PDF file includes:
Figs. S1 to S7
Tables S1 to S7
Legend for dataset S1

Other Supplementary Material for this manuscript includes the following:
Dataset S1

REFERENCES AND NOTES

1. A. Stevenson, J. A. Cray, J. P. Williams, R. Santos, R. Sahay, N. Neuenkirchen, C. D. McClure, I. R. Grant, J. D. Houghton, J. P. Quinn, D. J. Timson, S. V. Patil, R. S. Singhal, J. Antón, J. Dijksterhuis, A. D. Hocking, B. Lievens, D. E. N. Rangel, M. A. Voytek, N. Gunde-Cimerman, A. Oren, K. N. Timmis, T. J. McGenity, J. E. Hallsworth, Is there a common water-activity limit for the three domains of life? *ISME J.* **9**, 1333–1351 (2015).

2. W. D. Grant, Life at low water activity. *Philos. Trans. R. Soc. Lond. B Biol. Sci.* **359**, 1249–1267 (2004).

3. A. Oren, Thermodynamic limits to microbial life at high salt concentrations. *Environ. Microbiol.* **13**, 1908–1923 (2011).

4. J. P. Williams, J. E. Hallsworth, Limits of life in hostile environments: No barriers to biosphere function? *Environ. Microbiol.* **11**, 3292–3308 (2009).

5. A. Stevenson, P. G. Hamill, C. J. O'Kane, G. Kminek, J. D. Rummel, M. A. Voytek, J. Dijksterhuis, J. E. Hallsworth, Aspergillus penicillioides differentiation and cell division at 0.585 water activity. *Environ. Microbiol.* **19**, 687–697 (2017).

6. M. S. Tapia, S. M. Alzamora, J. Chirife, "Effects of water activity (a_w) on microbial stability as a hurdle in food preservation" in *Water Activity in Foods*, G. V. Barbosa-Cánovas, A. J. Fontana, S. J. Schmidt, T. P. Labuza, Eds. (Wiley, ed. 1, 2020), pp. 323–355.

7. W. D. Williams, Environmental threats to salt lakes and the likely status of inland saline ecosystems in 2025. *Environ. Conserv.* **29**, 154–167 (2002).

8. E. Kintisch, Record salinity and low water imperil Great Salt Lake. *Science* **377**, 1248–1249 (2022).

9. P. Rettberg, A. M. Anesio, V. R. Baker, J. A. Baross, S. L. Cady, E. Detsis, C. M. Foreman, E. Hauber, G. G. Ori, D. A. Pearce, N. O. Renno, G. Ruvkun, B. Sattler, M. P. Saunders, D. H. Smith, D. Wagner, F. Westall, Planetary protection and mars special regions—A suggestion for updating the definition. *Astrobiology* **16**, 119–125 (2016).

10. J. E. Hallsworth, R. L. Mancinelli, C. A. Conley, T. D. Dallas, T. Rinaldi, A. F. Davila, K. C. Benison, A. Rapoport, B. Cavalazzi, L. Selbmann, H. Changela, F. Westall, M. M. Yakimov, R. Amils, M. T. Madigan, Astrobiology of life on Earth. *Environ. Microbiol.* **23**, 3335–3344 (2021).

11. A. Stevenson, P. G. Hamill, Á. Medina, G. Kminek, J. D. Rummel, J. Dijksterhuis, D. J. Timson, N. Magan, S. L. Leong, J. E. Hallsworth, Glycerol enhances fungal germination at the water-activity limit for life. *Environ. Microbiol.* **19**, 947–967 (2017).

12. E. Nevoigt, U. Stahl, Osmoregulation and glycerol metabolism in the yeast Saccharomyces cerevisiae. *FEMS Microbiol. Rev.* **21**, 231–241 (1997).

13. A. Oren, Glycerol metabolism in hypersaline environments. *Environ. Microbiol.* **19**, 851–863 (2017).

14. J. E. Hallsworth, M. M. Yakimov, P. N. Golyshin, J. L. M. Gillion, G. D'Auria, F. D. L. Alves, V. La Cono, M. Genovese, B. A. McKew, S. L. Hayes, G. Harris, L. Giuliano, K. N. Timmis, T. J. McGenity, Limits of life in MgCl₂-containing environments: Chaotropicity defines the window. *Environ. Microbiol.* **9**, 801–813 (2007).

15. M. M. Yakimov, V. La Cono, G. L. Spada, G. Bortoluzzi, E. Messina, F. Smedile, E. Arcadi, M. Borghini, M. Ferrer, P. Schmitt-Kopplin, N. Hertkorn, J. A. Cray, J. E. Hallsworth, P. N. Golyshin, L. Giuliano, Microbial community of the deep-sea brine Lake Kryos seawater-brine interface is active below the chaotropicity limit of life as revealed by recovery of mRNA. *Environ. Microbiol.* **17**, 364–382 (2015).

16. V. I. Duda, V. N. Danilevich, N. E. Suzina, A. P. Shorokhova, V. V. Dmitriev, O. N. Mokhova, V. N. Akimov, Changes in the fine structure of microbial cells induced by chaotropic salts. *Microbiology* **73**, 341–349 (2004).

17. B. Klempay, N. Arandia-Gorostidi, A. E. Dekas, D. H. Bartlett, C. E. Carr, P. T. Doran, A. Dutta, N. Erazo, L. A. Fisher, J. B. Glass, A. Pontefract, S. M. Som, J. M. Wilson, B. E. Schmidt, J. S. Bowman, Microbial diversity and activity in Southern California salterns and bitterns: Analogues for remnant ocean worlds. *Environ. Microbiol.* **23**, 3825–3839 (2021).

18. M. Neveu, L. E. Hays, M. A. Voytek, M. H. New, M. D. Schulte, The ladder of life detection. *Astrobiology* **18**, 1375–1402 (2018).

19. J. Henry, E. Sun, I. Friedmann, Growth on geological time scales in the antarctic cryptoendolithic microbial community. *Geomicrobiol. J.* **16**, 193–202 (1999).

20. M. R. Mormile, B.-Y. Hong, K. C. Benison, Molecular analysis of the microbial communities of Mars analog lakes in Western Australia. *Astrobiology* **9**, 919–930 (2009).

21. H. D. Dickins, E. S. Van Vleet, Archaebacterial activity in the Orca Basin determined by the isolation of characteristic isopranyl ether-linked lipids. *Deep Sea Res.* **39**, 521–536 (1992).

22. P. A. LaRock, R. D. Lauer, J. R. Schwarz, K. K. Watanabe, D. A. Wiesenburg, Microbial biomass and activity distribution in an anoxic, hypersaline basin. *Appl. Environ. Microbiol.* **37**, 466–470 (1979).

23. S. Borin, E. Crotti, F. Mapelli, I. Tamagnini, C. Corselli, D. Daffonchio, DNA is preserved and maintains transforming potential after contact with brines of the deep anoxic hypersaline lakes of the Eastern Mediterranean Sea. *Saline Syst.* **4**, 10 (2008).

24. C. Corinaldesi, M. Tangherlini, G. M. Luna, A. Dell'Anno, Extracellular DNA can preserve the genetic signatures of present and past viral infection events in deep hypersaline anoxic basins. *Proc. Biol. Sci.* **281**, 20133299 (2014).

25. S. Bairoliya, J. K. Z. Xiang, B. Cao, Extracellular DNA in environmental samples: Occurrence, extraction, quantification, and impact on microbial biodiversity assessment. *Appl. Environ. Microbiol.* **88**, e0184521 (2022).

26. B. J. Tuovila, F. C. Dobbs, P. A. LaRock, B. Z. Siegel, Preservation of ATP in hypersaline environments. *Appl. Environ. Microbiol.* **53**, 2749–2753 (1987).

27. I. Joint, P. Henriksen, K. Garde, B. Riemann, Primary production, nutrient assimilation and microzooplankton grazing along a hypersaline gradient. *FEMS Microbiol. Ecol.* **39**, 245–257 (2002).

28. N. Arandia-Gorostidi, A. E. Parada, A. E. Dekas, Single-cell view of deep-sea microbial activity and intracommunity heterogeneity. *ISME J.* **17**, 59–69 (2023).

29. P. Narasingarao, S. Podell, J. A. Ugalde, C. Brochier-Armanet, J. B. Emerson, J. J. Brocks, K. B. Heidelberg, J. F. Banfield, E. E. Allen, De novo metagenomic assembly reveals abundant novel major lineage of Archaea in hypersaline microbial communities. *ISME J.* **6**, 81–93 (2012).

30. B. Rodriguez-Brito, L. Li, L. Wegley, M. Furlan, F. Angly, M. Breitbart, J. Buchanan, C. Desnues, E. Dinsdale, R. Edwards, B. Felts, M. Haynes, H. Liu, D. Lipson, J. Mahaffy, A. B. Martin-Cuadrado, A. Mira, J. Nulton, L. Pašić, S. Rayhawk, J. Rodriguez-Mueller, F. Rodriguez-Valera, P. Salamon, S. Srinagesh, T. F. Thingstad, T. Tran, R. V. Thurber, D. Willner, M. Youle, F. Rohwer, Viral and microbial community dynamics in four aquatic environments. *ISME J.* **4**, 739–751 (2010).

31. E. A. Dinsdale, R. A. Edwards, D. Hall, F. Angly, M. Breitbart, J. M. Brulc, M. Furlan, C. Desnues, M. Haynes, L. Li, L. McDaniel, M. A. Moran, K. E. Nelson, C. Nilsson, R. Olson, J. Paul, B. R. Brito, Y. Ruan, B. K. Swan, R. Stevens, D. L. Valentine, R. V. Thurber, L. Wegley, B. A. White, F. Rohwer, Functional metagenomic profiling of nine biomes. *Nature* **452**, 629–632 (2008).

32. O. Zhaxybayeva, R. Stepanauskas, N. R. Mohan, R. T. Papke, Cell sorting analysis of geographically separated hypersaline environments. *Extremophiles* **17**, 265–275 (2013).

33. K. Bidle, W. Amadio, P. Oliveira, T. Paulish, S. Hicks, C. Earnest, Research article: A phylogenetic analysis of haloarchaea found in a solar saltern. *Bios* **76**, 89–96 (2005).

34. A. E. Dekas, A. E. Parada, X. Mayali, J. A. Fuhrman, J. Wollard, P. K. Weber, P. Pett-Ridge, Characterizing chemoautotrophy and heterotrophy in marine archaea and bacteria with single-cell multi-isotope NanoSIP. *Front. Microbiol.* **10**, 2682 (2019).

35. X. Mayali, P. K. Weber, J. Pett-Ridge, Taxon-specific C/N relative use efficiency for amino acids in an estuarine community. *FEMS Microbiol. Ecol.* **83**, 402–412 (2013).

36. C. Gini, *Variabilità e Mutabilità: Contributo Allo Studio Delle Distribuzioni e Delle Relazioni Statistiche. [Fasc. I.] Studi economico-giuridici pubblicati per cura della facoltà di Giurisprudenza della R.* (Università di Cagliari, Tipogr. di P. Cuppini, 1912).

37. T. J. Wolery, EQ3/6 - Software for Geochemical Modeling, version 8.0a, Lawrence Livermore National Laboratory (2013).

38. C. M. Duarte, Y. T. Prairie, C. Montes, J. J. Cole, R. Striegl, J. Melack, J. A. Downing, CO_2 emissions from saline lakes: A global estimate of a surprisingly large flux. *J. Geophys. Res. Biogeo.* **113**, G04041 (2008).

39. L. A. Fisher, A. Pontefract, S. M. Som, C. E. Carr, B. Klempay, B. E. Schmidt, J. S. Bowman, D. H. Bartlett, Current state of athalassohaline deep-sea hypersaline anoxic basin research—recommendations for future work and relevance to astrobiology. *Environ. Microbiol.* **23**, 3360–3369 (2021).

40. N. O. Renno, E. Fischer, G. Martínez, J. Hanley, Complex brines and their Implications for habitability. *Life (Basel)* **11**, 847 (2021).

41. J. Heinz, J. Schirmack, A. Airo, S. P. Kounaves, D. Schulze-Makuch, Enhanced microbial survivability in subzero brines. *Astrobiology* **18**, 1171–1180 (2018).

42. A. Kurt-Kızıldoğan, B. Abanoz, S. Okay, Global transcriptome analysis of Halolamina sp. to decipher the salt tolerance in extremely halophilic archaea. *Gene* **601**, 56–64 (2017).

43. R. Karan, M. D. Capes, S. DasSarma, Function and biotechnology of extremophilic enzymes in low water activity. *Aquat. Biosyst.* **8**, 4 (2012).

44. N. I. Dmitrieva, K. Cui, D. A. Kitchaev, K. Zhao, M. B. Burg, DNA double-strand breaks induced by high NaCl occur predominantly in gene deserts. *Proc. Natl. Acad. Sci.* **108**, 20796–20801 (2011).

45. M. G. Fox-Powell, J. E. Hallsworth, C. R. Cousins, C. S. Cockell, Ionic strength is a barrier to the habitability of Mars. *Astrobiology* **16**, 427–442 (2016).

46. S. J. Payler, J. F. Biddle, B. Sherwood Lollar, M. G. Fox-Powell, T. Edwards, B. T. Ngwenya, S. M. Paling, C. S. Cockell, An ionic limit to life in the deep subsurface. *Front. Microbiol.* **10**, 426 (2019).

47. K. B. Sørensen, D. E. Canfield, A. Oren, Salinity responses of benthic microbial communities in a solar saltern (Eilat, Israel). *Appl. Environ. Microbiol.* **70**, 1608–1616 (2004).

48. D. M. Voica, L. Bartha, H. L. Banciu, A. Oren, Heavy metal resistance in halophilic *Bacteria* and *Archaea*. *FEMS Microbiol. Lett.* **363**, fnw146 (2016).

49. J. K. Apple, P. A. del Giorgio, Organic substrate quality as the link between bacterioplankton carbon demand and growth efficiency in a temperate salt-marsh estuary. *ISME J.* **1**, 729–742 (2007).

50. M. Bonete, R. Martínez-Espinosa, C. Pire, B. Zafrilla, D. J. Richardson, Nitrogen metabolism in haloarchaea. *Saline Syst.* **4**, 9 (2008).

51. S. A. Bursakov, C. Carneiro, M. J. Almendra, R. O. Duarte, F. J. F. Caldeira, I. Moura, J. J. G. Moura, Enzymatic properties and effect of ionic strength on periplasmic nitrate reductase (NAP) from *Desulfovibrio desulfuricans* ATCC 27774. *Biochem. Biophys. Res. Commun.* **239**, 816–822 (1997).

52. S. K. Hemida, S. A. Omar, A. Y. Abdel-Mallek, Microbial populations and enzyme activity in soil treated with heavy metals. *Water Air Soil Pollut.* **95**, 13–22 (1997).

53. M. B. Burg, J. D. Ferraris, Intracellular organic osmolytes: Function and regulation. *J. Biol. Chem.* **283**, 7309–7313 (2008).

54. A. Braun, M. Spona-Friedl, M. Avramov, M. Elsner, F. Baltar, T. Reinthaler, G. J. Herndl, C. Griebler, Reviews and syntheses: Heterotrophic fixation of inorganic carbon – significant but invisible flux in environmental carbon cycling. *Biogeosciences* **18**, 3689–3700 (2021).

55. R. Elevi Bardavid, P. Khristo, A. Oren, Interrelationships between Dunaliella and halophilic prokaryotes in saltern crystallizer ponds. *Extremophiles* **12**, 5–14 (2008).

56. M. G. Fox-Powell, C. S. Cockell, Building a geochemical view of microbial salt tolerance: Halophilic adaptation of marinococcus in a natural magnesium sulfate brine. *Front. Microbiol.* **9**, 739 (2018).

57. J. Belilla, D. Moreira, L. Jardillier, G. Reboul, K. Benzerara, J. M. López-García, P. Bertolino, A. I. López-Archilla, P. López-García, Hyperdiverse archaea near life limits at the polyextreme geothermal Dallol area. *Nat. Ecol. Evol.* **3**, 1552–1561 (2019).

58. A. Stevenson, P. G. Hamill, J. Dijksterhuis, J. E. Hallsworth, Water-, pH- and temperature relations of germination for the extreme xerophiles Xeromyces bisporus (FRR 0025), Aspergillus penicillioides (JH06THJ) and Eurotium halophilicum (FRR 2471). *Microbial. Biotechnol.* **10**, 330–340 (2017).

59. N. R. Meyer, J. Fortney, A. E. Dekas, NanoSIMS sample preparation decreases isotope enrichment: Magnitude, variability and implications for single-cell rates of microbial activity. *Environ. Microbiol.* **23**, 81–98 (2021).

60. M. F. Roberts, Organic compatible solutes of halotolerant and halophilic microorganisms. *Saline Syst.* **1**, 5 (2005).

61. A. Oren, Life at high salt concentrations, intracellular KCl concentrations, and acidic proteomes. *Front. Microbiol.* **4**, 315 (2013).

62. N. Gunde-Cimerman, A. Plemenitaš, A. Oren, Strategies of adaptation of microorganisms of the three domains of life to high salt concentrations. *FEMS Microbiol. Rev.* **42**, 353–375 (2018).

63. F. Schreiber, M. Ackermann, Environmental drivers of metabolic heterogeneity in clonal microbial populations. *Curr. Opin. Biotechnol.* **62**, 202–211 (2020).

64. F. Schreiber, S. Littmann, G. Lavik, S. Escrig, A. Meibom, M. M. M. Kuypers, M. Ackermann, Phenotypic heterogeneity driven by nutrient limitation promotes growth in fluctuating environments. *Nat. Microbiol.* **1**, 16055 (2016).

65. A. Stevenson, J. Burkhardt, C. S. Cockell, J. A. Cray, J. Dijksterhuis, M. Fox-Powell, T. P. Kee, G. Kminek, T. J. McGenity, K. N. Timmis, D. J. Timson, M. A. Voytek, F. Westall, M. M. Yakimov, J. E. Hallsworth, Multiplication of microbes below 0.690 water activity: Implications for terrestrial and extraterrestrial life. *Environ. Microbiol.* **17**, 257–277 (2015).

66. F. de Lima Alves, A. Stevenson, E. Baxter, J. L. M. Gillion, F. Hejazi, S. Hayes, I. E. G. Morrison, B. A. Prior, T. J. McGenity, D. E. N. Rangel, N. Magan, K. N. Timmis, J. E. Hallsworth, Concomitant osmotic and chaotropicity-induced stresses in Aspergillus wentii: Compatible solutes determine the biotic window. *Curr. Genet.* **61**, 457–477 (2015).

67. J. E. Hallsworth, S. Heim, K. N. Timmis, Chaotropic solutes cause water stress in Pseudomonas putida. *Environ. Microbiol.* **5**, 1270–1280 (2003).

68. J. D. Crisler, F. Chen, B. C. Clark, M. A. Schneegurt, Cultivation and characterization of the bacterial assemblage of epsomic Basque Lake, BC. *Antonie Van Leeuwenhoek* **112**, 1105–1119 (2019).

69. L. Steinle, K. Knittel, N. Felber, C. Casalino, G. de Lange, C. Tessarolo, A. Stadnitskaia, J. S. Sinninghe Damsté, J. Zopfi, M. F. Lehmann, T. Treude, H. Niemann, Life on the edge: Active microbial communities in the Kryos $MgCl_2$-brine basin at very low water activity. *ISME J.* **12**, 1414–1426 (2018).

70. L. Ojha, M. B. Wilhelm, S. L. Murchie, A. S. McEwen, J. J. Wray, J. Hanley, M. Massé, M. Chojnacki, Spectral evidence for hydrated salts in recurring slope lineae on Mars. *Nat. Geosci.* **8**, 829–832 (2015).

71. J. J. Buffo, B. E. Schmidt, C. Huber, C. C. Walker, Entrainment and dynamics of ocean-derived impurities within Europa's ice shell. *J. Geophys. Res. Planets* **125**, e2020JE006394 (2020).

72. N. S. Wolfenbarger, M. G. Fox-Powell, J. J. Buffo, K. M. Soderlund, D. D. Blankenship, Brine volume fraction as a habitability metric for Europa's ice shell. *Geophys. Res. Lett.* **49**, e2022GL100586 (2022).

73. G. Tobie, O. Choukroun, O. Grasset, S. Le Mouélic, J. I. Lunine, C. Sotin, O. Bourgeois, D. Gautier, M. Hirtzig, S. Lebonnois, L. Le Corre, Evolution of titan and implications for its hydrocarbon cycle. *Philos. Trans. A Math. Phys. Eng. Sci.* **367**, 617–631 (2009).

74. C. R. Glein, J. A. Baross, J. H. Waite, The pH of Enceladus' ocean. *Geochim. Cosmochim. Acta* **162**, 202–219 (2015).

75. T. R. Parsons, Y. Maita, C. M. Lalli, "Determination of dissolved free amino acids by fluorometric analysis" in *A Manual of Chemical & Biological Methods for Seawater Analysis*, T. R. Parsons, Y. Maita, C. M. Lalli, Eds. (Pergamon Press, 1984), pp. 40–44.

76. E. García-Robledo, A. Corzo, S. Papaspyrou, A fast and direct spectrophotometric method for the sequential determination of nitrate and nitrite at low concentrations in small volumes. *Mar. Chem.* **162**, 30–36 (2014).

77. J. D. H. Strickland, T. R. Parsons, *A Practical Handbook of Sea-Water Analysis* (Fisheries Research Board of Canada, ed. 2, 1972), vol. 167.

78. R. Benner, M. Strom, A critical evaluation of the analytical blank associated with DOC measurements by high-temperature catalytic oxidation. *Mar. Chem.* **41**, 153–160 (1993).

79. K. Grasshoff, K. Kremling, M. Ehrhardt, Eds., *Methods of Seawater Analysis* (John Wiley & Sons, ed. 1, 1999).

80. W. Walters, E. R. Hyde, D. Berg-Lyons, G. Ackermann, G. Humphrey, A. Parada, J. A. Gilbert, J. K. Jansson, J. G. Caporaso, J. A. Fuhrman, A. Apprill, R. Knight, Improved bacterial 16S rRNA gene (V4 and V4-5) and fungal internal transcribed spacer marker gene primers for microbial community surveys. *mSystems* **1**, e00009–e00015 (2015).

81. B. J. Callahan, P. J. McMurdie, M. J. Rosen, A. W. Han, A. J. A. Johnson, S. P. Holmes, DADA2: High-resolution sample inference from Illumina amplicon data. *Nat. Methods* **13**, 581–583 (2016).

82. J. S. Bowman, H. W. Ducklow, Microbial communities can be described by metabolic structure: A general framework and application to a seasonally variable, depth-stratified microbial community from the coastal west Antarctic peninsula. *PLOS ONE* **10**, e0135868 (2015).

83. J. Pett-Ridge, P. K. Weber, NanoSIP: NanoSIMS applications for microbial biology. *Methods Mol. Biol.* **881**, 375–408 (2022).

84. L. Polerecky, B. Adam, J. Milucka, N. Musat, T. Vagner, M. M. M. Kuypers, Look@NanoSIMS - a tool for the analysis of nanoSIMS data in environmental microbiology. *Environ. Microbiol.* **14**, 1009–1023 (2012).

85. S. Behrens, T. Lösekann, J. Pett-Ridge, P. K. Weber, W. O. Ng, B. S. Stevenson, I. D. Hutcheon, D. A. Relman, A. M. Spormann, Linking microbial phylogeny to metabolic activity at the single-cell level by using enhanced element labeling-catalyzed reporter deposition fluorescence in situ hybridization (EL-FISH) and NanoSIMS. *Appl. Environ. Microbiol.* **74**, 3143–3150 (2008).

86. G. Muller-Parker, C. B. Cook, C. F. D'Elia, Elemental composition of the coral pocillopora damicornis exposed to elevated seawater ammonium. *Pac. Sci.* **48**, 234–246 (1994).

87. C. Panagiotopoulos, M. Pujo-Pay, M. Benavides, F. Van Wambeke, R. Sempéré, The composition and distribution of semi-labile dissolved organic matter across the southwest Pacific. *Biogeosciences* **16**, 105–116 (2019).

88. H. Sakugawa, N. Handa, Chemical studies of dissolved carbohydrates in seawater. *J. Oceanogr. Soc. Japan* **39**, 279–288 (1983).

89. R. Fukuda, H. Ogawa, T. Nagata, I. Koike, Direct determination of carbon and nitrogen contents of natural bacterial assemblages in marine environments. *Appl. Environ. Microbiol.* **64**, 3352–3358 (1998).

90. A. Signorell, et al., DescTools: Tools for descriptive statistics. R package version 0.99.23., (2017).

91. A. E. Parada, X. Mayali, P. K. Weber, J. Wollard, A. E. Santoro, J. A. Fuhrman, J. Pett-Ridge, A. E. Dekas, Constraining the composition and quantity of organic matter used by abundant marine Thaumarchaeota. *Environ. Microbiol.* **25**, 689–704 (2023).

92. K. R. Clarke, Non-parametric multivariate analyses of changes in community structure. *Aust. J. Ecol.* **18**, 117–143 (1993).

93. H. Wickham, *ggplot2: Elegant Graphics for Data Analysis* (Springer-Verlag New York, 2016).